ISSN (Print) 1226-1750
ISSN (Online) 2233-6656
Journal of Magnetics 20(4), 353-359 (2015) http://dx.doi.org/10.4283/JMAG.2015.20.4.353

Relaxor Behaviors in xBaTiO$_3$–(1-x)CoFe$_2$O$_4$ Materials

Cao Thi My Dung[1,a], Nhu Hoa Tran Thi[1,2,a], Kieu Hanh Thi Ta[1], Vinh Cao Tran[3], Bao Thu Le Nguyen[4], Van Hieu Le[1], Phuong Anh Do[5], Anh Tuan Dang[5], Heongkyu Ju[2], and Bach Thang Phan[1,3,*]

[a]*Ms. Dung and Ms. Hoa contributed equally to this work.*
[1]*Faculty of Materials Science, University of Science, Vietnam National University, Ho Chi Minh City, Viet Nam*
[2]*Department of Nano-Physics, Gachon University, Seongnam-city 461-701, Korea*
[3]*Laboratory of Advanced Materials, University of Science, Vietnam National University, Ho Chi Minh City, Viet Nam*
[4]*Department of Mathematics and Physics, University of Information Technology, Vietnam National University, Ho Chi Minh City, Viet Nam*
[5]*Department of Solid State Physics, Faculty of Physics, Hue University, Vietnam*

(Received 11 September 2015, Received in final form 9 December 2015, Accepted 9 December 2015)

Dielectric properties of xBaTiO$_3$–(1-x)CoFe$_2$O$_4$ composite materials have been investigated. Dielectric properties of BaTiO$_3$, CoFe$_2$O$_4$ and 0.5BaTiO$_3$–0.5CoFe$_2$O$_4$ samples show frequency dependence, which is classified as relaxor behavior with different relaxing degree. The relaxor behaviors were described using the modified Curier-Weiss and Vogel–Fulcher laws. Among three above samples, the BaTiO$_3$ sample has highest relaxing degree. Photoluminescence spectral indicated defects, which might in turn control relaxing degree.

Keywords : xBaTiO$_3$–(1-x)CoFe$_2$O$_4$, dielectric properties, relaxing degree, modified Curie-Weiss law, Vogel-Fulcher law

1. Introduction

Relaxor materials, such as ferroelectric materials, have found a vast range of application in electronics, electro-mechanics, optoelectronics and others, because of their large dielectric, pyroelectric, piezoelectric and electro-optic properties [1]. Difference between normal ferro-electrics and relaxor ferroelectrics can be described by three qualitatively distinguished features: (a) diffuse phase transition (DPT) extended in a large range of temperatures; (b) a non-Debye dielectric dispersion in the polar phase and frequency-independent dielectric constant in the paraelectric state; (c) Curie-Weiss dependence of the permittivity shows strong deviations at temperatures above maximum temperature T_m ($T \geq T_m$)… [2]. Most of the relaxor materials are lead-based materials, such as Pb(Mg$_{1/3}$Nb$_{2/3}$)O$_3$, Pb(Fe$_{1/2}$Nb$_{1/2}$)O$_3$, 0.8Pb(Fe$_{2/3}$W$_{1/3}$)O$_3$–0.2PbTiO$_3$, and 0.8Pb(Fe$_{1/2}$Nb$_{1/2}$)O$_3$–0.2Pb(Mg$_{1/2}$W$_{1/2}$)O$_3$ [1, 3-9]. Since the disadvantages of lead-based materials are the volatility and toxicity of PbO, recent research emphasis is leaning towards environmental friendly lead-free oxides, such as barium-based relaxors. Barium Titanate (BaTiO$_3$), as a member of perovskite family, is a normal ferroelectric material with large piezoelectricy. It is usually agreed that microscopic compositional inhomogeneity is an essential feature of relaxor ferroelectrics, e.g. the homovalent substitution in the B-site (BaTi$_{1-x}$B$_x$O$_3$; B = Sn, Ce, Zr) can switch normal ferroelectric BaTiO$_3$ to relaxor ferroelectric [1, 10]. It is well known that CoFe$_2$O$_4$ belongs to the family of spinels, a ferrimagnetic with large magnetostriction. Correlation between normal ferroelectric (BaTiO$_3$) and magnetic order (CoFe$_2$O$_4$) control magnetoelectric effect in multiferroic BaTiO$_3$–CoFe$_2$O$_4$ composite materials [11-16]. Both the BaTiO$_3$ and CoFe$_2$O$_4$ phases in BaTiO$_3$–CoFe$_2$O$_4$ composite materials mutually affect each other, in turn controlling properties of the BaTiO$_3$–CoFe$_2$O$_4$ composites. In this study, we report the relaxor behaviors in the BaTiO$_3$, CoFe$_2$O$_4$ and 0.5BaTiO$_3$–0.5CoFe$_2$O$_4$ composite materials. It is well known that BaTiO$_3$ is not a typical relaxor. The homovalent substitution in the B-site of BTO with Sn, Ce, Zr can switch BaTiO$_3$ from normal ferroelectric to relaxor ferroelectric, but our obtained data shows an abnormal behavior, in which BaTiO$_3$ has the strongest relaxor behavior in the samples studied. Photoluminescence spectral indicated intrinsic defects, which might induce that

©The Korean Magnetics Society. All rights reserved.
*Corresponding author: Tel: +84-83-835-0831
Fax: +84-83-835-0831, e-mail: pbthang@hcmus.edu.vn

© 2015 Journal of Magnetics

abnormal behavior.

2. Experimentals

Ferrite–ferroelectric xBaTiO$_3$–(1-x)CoFe$_2$O$_4$ composite materials with various volume fraction x (0, 0.5, and 1) were synthesized by simplified solid-state reaction processes. The oxide powders were mixed in ethanol and zirconia grinding media for 5 hours then dried at 80 °C in 24 hours. After CoFe$_2$O$_4$ and BaTiO$_3$ powders has been prepared, they were mixed with volume fraction x of 0.5. The samples were compressed into pellets form with diameter of 10 mm and thickness of 1.5 mm using an applied pressure of 69 MPa (~10000 psi). The pellets were presintered at 1100 °C and followed by the sintering at higher temperature of 1200 °C for 24 h in air with a heating rate of 2 °C/min. The microstructure and crystalline phases of the composite samples were investigated by scanning electron microscopy (Hitachi FESEM, S-4800) and X-ray diffractometer (XRD, D8 Advance Bruker) with Cu K$_\alpha$ radiation (λ = 0.154 nm), respectively. A vibrating sample magnetometer (VSM) was employed to measure magnetic properties of the composite samples. Dielectric properties of the composite samples were carried out using RLC (HIOKI 3532) system. The room-temperature photoluminescence (PL) spectra were examined using excitation wavelength of 488 nm.

3. Results and Discussions

Figure 1 shows XRD patterns of single BaTiO$_3$ (BTO), CoFe$_2$O$_4$ (CFO) and 0.5BaTiO$_3$–0.5CoFe$_2$O$_4$ (0.5BTO-0.5CFO) composite materials. Peaks located at 2θ = 22.19°, 31.58°, 38.93°, 45.32°, 50.99°, 56.21° and 65.77° are representative diffraction peaks of CoFe$_2$O$_4$ spinel structure, and the other peaks at 2θ = 30.07°, 35.5°, 43.18°, 53.77°, 57.13°, 62.71° are characteristics of perovskite BaTiO$_3$ structure. Both the CFO and BTO phases are polycrystalline with the preferentially crystallographic orientation of (110) and (311) for BTO and CFO phases, respectively. In the case of 0.5BaTiO$_3$–0.5CoFe$_2$O$_4$ composite materials, the XRD shows that the composite materials consist of both the CFO and BTO phases without any additional or intermediate phases. In

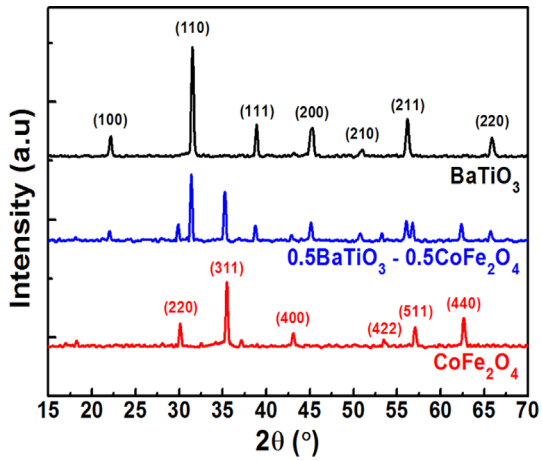

Fig. 1. (Color online) XRD pattern of xBaTiO$_3$–(1-x)CoFe$_2$O$_4$ composite materials with x = 1, 0.5 and 0.

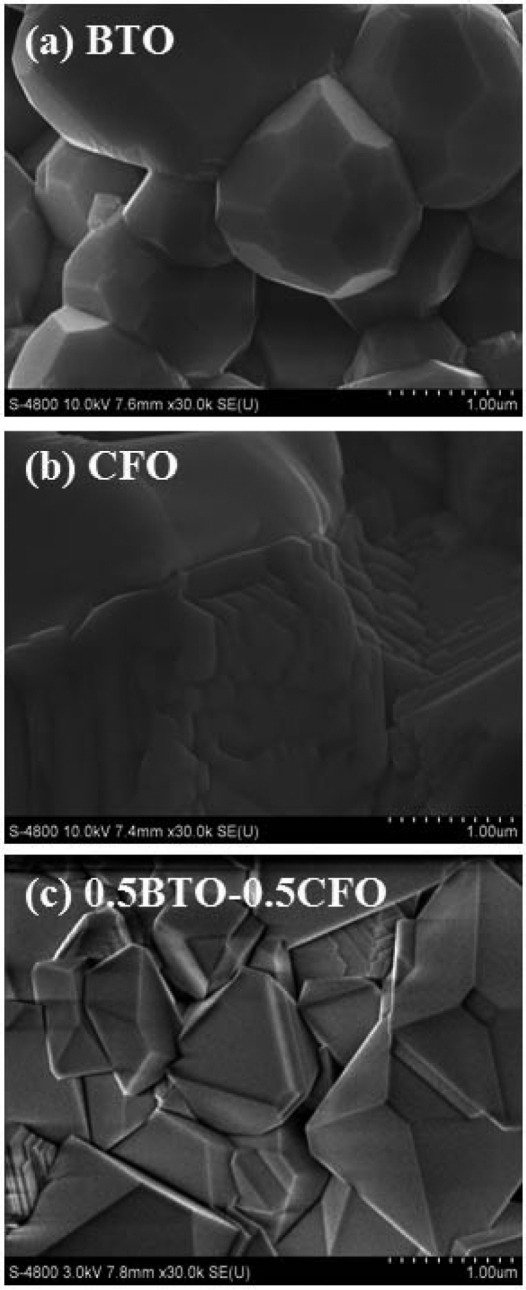

Fig. 2. SEM images of xBaTiO$_3$–(1-x)CoFe$_2$O$_4$ composite materials with x = 1, 0.5 and 0.

comparison, intensity of peak (110) is higher than intensity of (311) peak, indicating the dominant BTO phase over the CFO phase in the 0.5BTO–0.5CFO composite materials.

Figure 2 shows top-view SEM images of the morphology for BTO, CFO and 0.5BTO–0.5CFO composite samples. All samples show dense microstructures. It is observable that the BTO samples is formed with a clear polyhedron structure (Fig. 2a), while the CFO samples exhibit layer structure (Fig. 2b). The 0.5BTO–0.5CFO composite samples exhibit both the above characterization structures (Fig. 2c) with two dissimilar particle shapes corresponding to two different phases. Since we could distinctly observe the morphology of the BTO and CFO structures in the 0.5BTO–0.5CFO composite materials, this suggests that there are no diffusions at the interfaces between the BTO and CFO phases, which are consistent to the XRD data.

M-H curves of the BTO, CFO and 0.5BTO–0.5CFO samples measured at room temperature are shown in Fig. 3. Magnetic measurements of the BTO sample were performed showing diamagnetic properties (Fig. 3a), while the CFO and 0.5BTO–0.5CFO composited samples show hysteresis behavior, a characteristic of ferro/ferrimagnetism or spin glass (Fig. 3b). Magnetic measurements of the 0.5BTO–0.5CFO composite materials show that coercivity increases and magnetization saturation decreases with the increase of BTO content. The origin of hysteresis can be ascribed to canting of spins as the bond

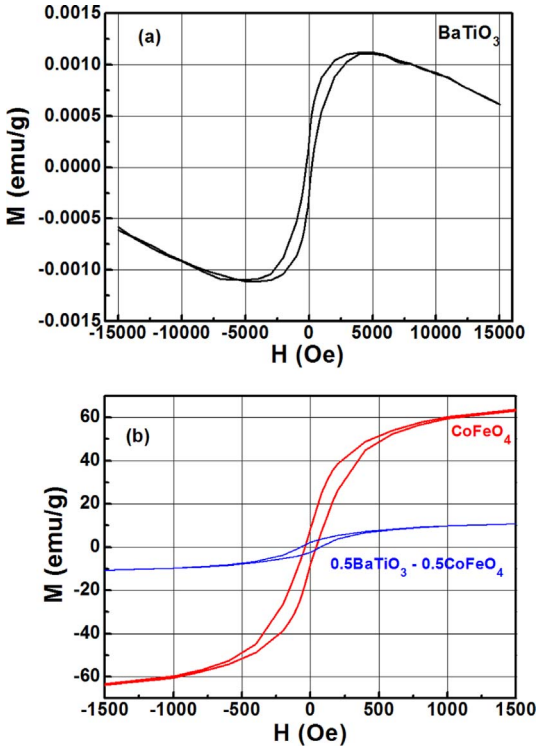

Fig. 3. (Color online) M-H curve of BTO, CFO and 0.5BaTiO_3 –0.5$CoFe_2O_4$ composite materials.

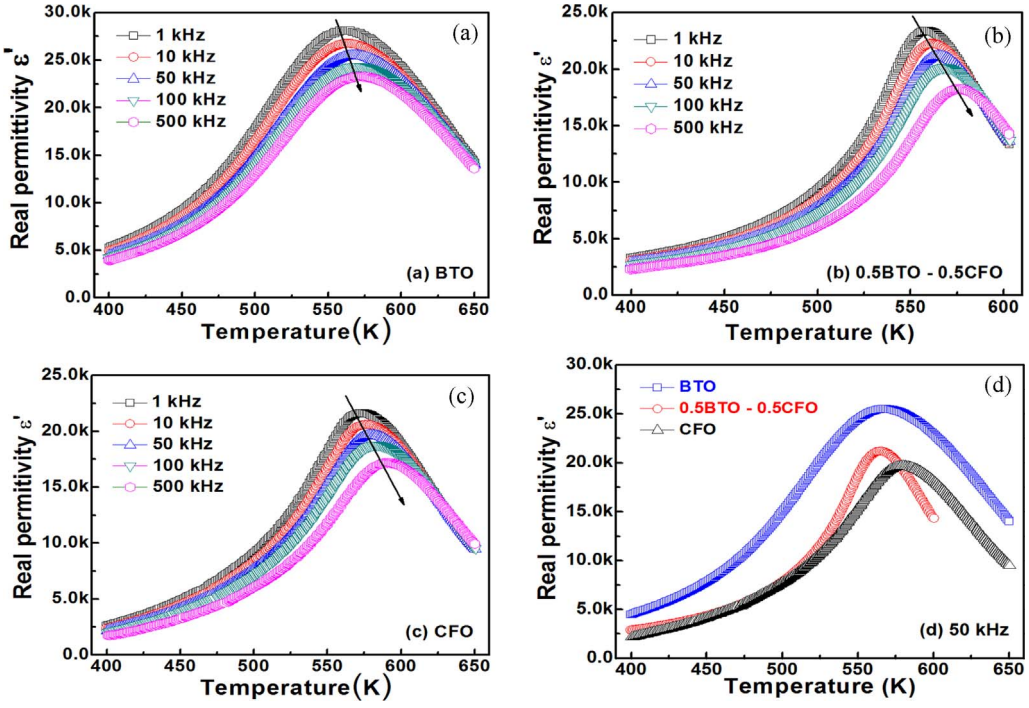

Fig. 4. (Color online) Temperature dependent dielectric spectra ε' of $xBaTiO_3$–(1-x)$CoFe_2O_4$ composite materials with x = 1, 0.5 and 0 at various frequencies.

angle of Fe–O–Fe changes. In addition, Fe^{2+} or oxygen vacancies may appear to compensate charge imbalance arising from the substitutions at A-sites and/or B-sites (Ba^{2+} by Co^{3+}, Ti^{4+} by Fe^{3+}), the distributions of Fe^{3+} and Fe^{2+} ions contribute to net magnetization.

Detail dielectric properties of the BTO, CFO and 0.5BTO–0.5CFO composite samples were characterized at various frequencies, 1 kHz–500 kHz, as shown in Fig. 4. Board peaks can be observed in the graph of real permittivity ε' versus T (Fig. 4a-c). Strong frequency dispersions below the maximum temperature (T'_m) are observed with a clear shift in the position of T'_m with

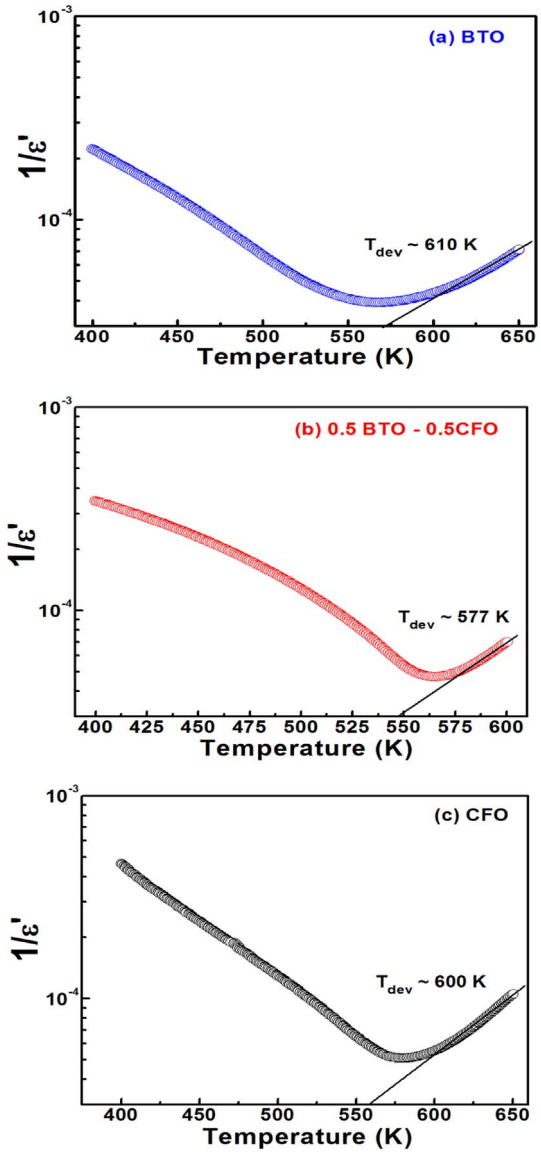

Fig. 5. (Color online) Dielectric properties ($1/\varepsilon'$ – T plot) measured at 50 kHz. Straight line shows the Curie-Weiss behavior of xBaTiO$_3$–(1-x)CoFe$_2$O$_4$ composite materials with x = 1, 0.5 and 0 at higher temperature.

Table 1. Fitting parameters extracted from figure 5 following Curie-Weiss law.

	T'_m (K)	T_{dev} (K)
BTO	568	610
0.5BTO–0.5CFO	565	577
CFO	580	600

frequencies. With increasing frequency, the T'_m position shifts to higher temperatures along with the decrease of maximum value of dielectric permittivity (real component ε'). These observations are typical features of relaxor materials. It is noted that the BTO sample has boarder dielectric peak while the 0.5BTO–0.5CFO sample has sharper dielectric peak. As shown in Fig. 4d.

In normal ferroelectric/ferromagnetic materials, the high temperature-dielectric behavior is described by the Curie-Weiss law ($T > T_{CW}$) [1, 17-21]

$$1/\varepsilon' = [T - T_{CW}]/C, \quad (1)$$

where C is the Curie-Weiss constant and T_{CW} is the Curie-Weiss temperature. The fitting of our data to the expression (1) is displayed in Fig. 5 for the measuring frequency of 50 kHz. The temperature T_{dev} where the data starts deviating from the Curie-Weiss law is defined and listed in Table 1.

Temperature-dielectric behavior in a temperature ranges above the peak temperature T'_m can be described using the modified Curie-Weiss relation [1, 17-21],

$$1/\varepsilon' - 1/\varepsilon'_m = [T - T'_m]^{\gamma}/C_1 \qquad 1 \le \gamma \le 2, \quad (2)$$

where ε' is the value of the permitivity at the temperature T while ε'_m is the value at the peak temperature T'_m. γ is the parameter regarding to the character of the phase transition (the degree of diffuseness) and C_1 is the modified Curie-Weiss constant. The value is 1 for normal

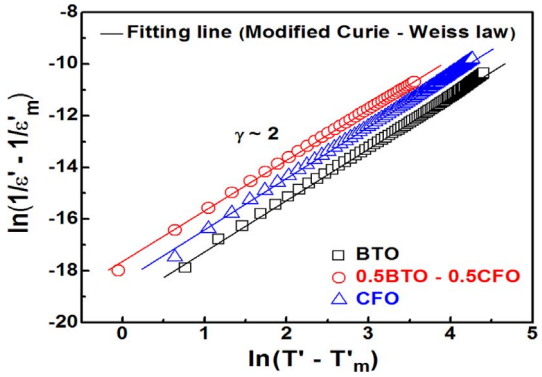

Fig. 6. (Color online) Modified Curier-Wiess law fitted for xBaTiO$_3$–(1-x)CoFe$_2$O$_4$ composite materials with x = 1, 0.5 and 0.

ferroelectrics, obeying the normal Curie-Weiss law. The γ value is reported to lie between 1 and 2 characterizing for relaxor materials, while γ equals 2 describing the completely diffuse phase transition. The mechanism of diffuse phase transition in ferroelectric materials is known to be generally associated with compositional inhomogeneity or other structural defects. Figure 6 shows a plot of $\ln[(1/\varepsilon') - (1/\varepsilon'_m)]$ versus $\ln(T-T'_m)$ at 50 kHz. By fitting the data using Eq. (2), the obtained g values are 2.0 for all investigated samples.

We now consider the behavior of the dielectric response below the peak temperature T'_m. The observed decrease of the dielectric permittivity at lower temperatures is typically associated with the freezing of the polar nano regions (PNRs). These regions are formed at elevated temperatures well above the peak temperature T'_m. This freezing is similar to spin glass freezing in magnetic systems where the spin may not have thermal energy enough to overcome competing interactions. The dielectric behavior of relaxors can be treated using the so-called Vogel-Fulcher relation [1, 17-21] in order to extract dynamic properties related to PNRS and the freezing temperature T_f.

$$f = f_o \exp\{-E_a/K_B[T'_m - T_f]\}, \quad (3)$$

where T_f is the static (f = 0) freezing temperature, E_a is the activation energy for polarization fluctuation of an isolated nano polar region, f_o is a characteristic attempt frequency, while T'_m is the peak temperature corresponding to the frequency f. The data for T'_m as a function of frequency f in the range of 1 to 500 kHz are shown in Fig. 7. The experiment points measured at 50 kHz fitted well with the Volgel-Fulcher relation (solid line). The fitting data are listed in Table 2. The degree of relaxation in the investigated materials can be classified through the temperature difference ΔT between T'_m and T_f. The BTO sample shows largest ΔT and activation energy E_a value

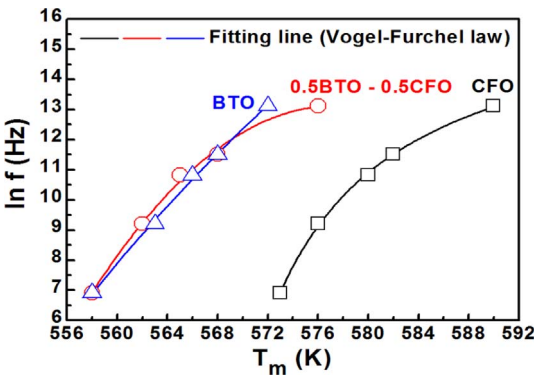

Fig. 7. (Color online) Vogel-Fulcher law fitted for xBaTiO$_3$–(1-x)CoFe$_2$O$_4$ composite materials with x = 1, 0.5 and 0.

Table 2. Fitting parameters extracted from figure 7 following Vogel-Fulcher law.

	T'_m (K)	T_f (K)	E_a (eV)	$\Delta T = T'_m - T_f$ (K)
BTO	568	469	0.354	99
0.5BTO–0.5CFO	565	544	0.013	21
CFO	580	562	0.009	18

indicating high relaxing degree. Although the 0.5BTO–0.5CFO sample has dominant BTO phase, its relaxing degree is the same as the CFO sample. This result suggests that the relaxor behavior in 0.5BTO–0.5CFO sample is significantly affected by the minor CFO phase. Future study is necessary to analyze this result.

The relaxor behavior in the investigated materials could be explained on the basis of a statistical compositional fluctuations and changes in distance of the adjacent ions due to lattice alteration (i.e., disorder in the arrangement of different ions on equivalent sites or oxygen vacancies in Co:Fe (CFO), Ba:Ti (BTO) and Ba:Fe:Co:Ti (0.5BTO–0.5CFO) concentrations). An inequivalent constituents can induce defects, such as A-site Co^{2+} substitutions together with the additional B-site Fe^{3+} substitutions, creating charge imbalance in the 0.5BTO–0.5CFO sample, which should be compensated by either A-site or B-site defects (cation vacancies or electrons), and/or the displacement of B-site ions (Ti) locating at the center of the unit cell. In addition, different degree of compositional fluctuation or defects induces different relaxing degree.

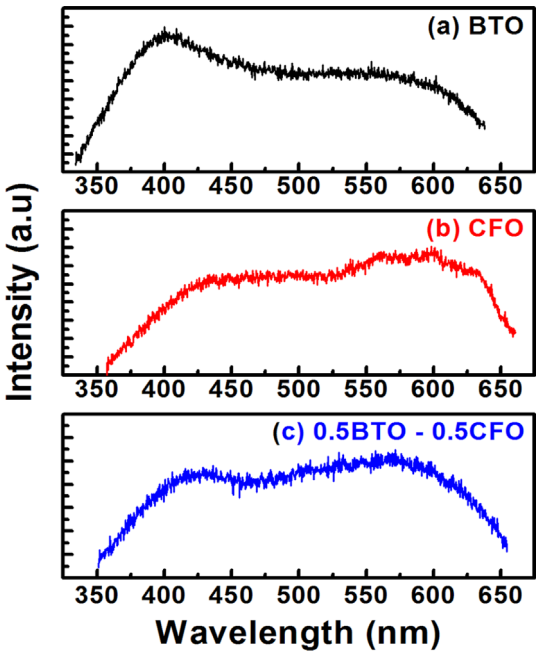

Fig. 8. (Color online) Photoluminescence spectral of xBaTiO$_3$–(1-x)CoFe$_2$O$_4$ composite materials with x = 1, 0.5 and 0.

Photoluminescence spectra, presented in Fig. 8, can provide valuable information on defects in the BTO, CFO and 0.5BTO–0.5CFO samples excited with 488 nm laser excitation at room temperature. The photoluminescence spectra (PL) of the CFO and 0.5BTO–0.5CFO samples were similar in shape with broad bands and were different from the photoluminescence spectra of the BTO sample: PL spectra of BTO sample consists of a strong violet emission around 405 nm and weak emission in the visible range, while PL spectra of the both CFO and 0.5BTO–0.5CFO samples consist of a weak violet emission and stronger specific emissions in the visible range.

Since the energy bandgap of bulk BTO sample is 2.9–3.4 eV, the strong violet emission is attributed to the recombination between electrons in the conduction band and holes in the valence band. The weak and broad visible emission is related to the intrinsic structural defects regarding to deep level emission or delocalized states in the bandgap, such as oxygen vacancies, non-central symmetric Ti^{3+} ... All these structural defects can give rise to a change in the octahedron configuration in the BTO. The flat and broad visible emission shows no clear emission peaks, resulting in an overlapping of a number of recombination channels related to some kind of intrinsic defects in the crystal structure of the BTO sample. The similar behavior was observed in our published report on ZnO films [22]. This case suggests that the BTO samples might have many kinds of defect and therefore its dielectric properties show high relaxing degree as discussed above.

For the CFO and 0.5BTO–0.5CFO samples, the visibly specific emissions with clearer emission peaks in the visible range are also related to the intrinsic structural defects. However, it seems that the defects were more specific and thus separated or clear emission peaks are observable. Consequently, the CFO and 0.5BTO–0.5CFO samples have lower relaxing degree.

4. Conclusions

In summary, the composite samples were synthesized by using a simplified solid-state reaction process. XRD patterns show that both the CFO and BTO phases are polycrystalline without any intermediate phases. The SEM images illustrate dense and clear microstructures of two $CoFe_2O_4$ and $BaTiO_3$ phases. The coercivity increases and the saturation magnetization decreases with the increase of BTO content. The dielectric properties with frequency dependence are typical features of relaxor materials, which are well described using both the modifiled Curier-Weiss and the Vogel–Fulcher laws. The BTO sample shows largest relaxing degree (largest ΔT and activation energy E_a) compared to the remaining samples. In this study, we report the relaxor behaviors in the $BaTiO_3$, $CoFe_2O_4$ and $0.5BaTiO_3$–$0.5CoFe_2O_4$ composite materials. It is well known that $BaTiO_3$ is not a typical relaxor but our obtained data shows an abnormal behavior, in which $BaTiO_3$ sample has the strongest relaxor behavior in the samples studied. Photoluminescence spectral indicated intrinsic defects, which might induce that abnormal behavior.

Acknowledgements

This work is financially supported by Vietnam National University in HoChiMinh City under Grant C2014-18-12.

References

[1] Tanmoy Maiti, PhD thesis, The Pennsylvania State University, USA (2007).
[2] L. Mitoseriu, D. Marré, A. S. Siri, A. Stancu, C. E. Fedor, and P. Nanni, J. Optoelectro, Adv. Mater. **6**, 723 (2004).
[3] A. A. Bokov and Z.-G. Ye, Phys. Rev. B **74**, 132102 (2006).
[4] J. Miao, X. G. Xu, Y. Jiang, and B. R. Zhao, Appl. Phys. Lett. **95**, 132905 (2009).
[5] L. Yan, J. F. Li, C. Suchicital, and D. Viehland, Appl. Phys. Lett. **89**, 132913 (2006).
[6] A. Kumar, I. Rivera, R. S. Katiyar, and J. F. Scott, Appl. Phys. Lett. **92**, 132913 (2008).
[7] W. Peng, N. Lemeé, J.-L. Dellis, V. V. Shvartsman, P. Borisov, W. Kleemann, Z. Trontelj, J. Holc, M. Kosec, R. Blinc, and M. G. Karkut, Appl. Phys. Lett. **95**, 132507 (2009).
[8] A. Levstik, V. Bobnar, C. Filipic, J. Holc, M. Kosec, R. Blinc, Z. Trontelj, and Z. Jaglicic, Appl. Phys. Lett. **91**, 012905 (2007).
[9] Z. Hu, T. Nan, X. Wang, M. Staruch, Y. Gao, P. Finkel, and N. X. Sun, Appl. Phys. Lett. **106**, 022901 (2015).
[10] C. E. Ciomaga, R. Calderone, M. T. Buscaglia, M. Viviani, V. Buscaglia, L. Mitoseriu, A. Stancu, and P. Nanni, J. Optoelec. Adv. Mater. **8**, 944 (2006).
[11] S. Q. Ren, L. Q. Weng, S. H. Song, F. Li, J. G. Wan, and M. Seng, J. Mater. Sci. **40**, 4375 (2005).
[12] J. X. Zhang, J. Y. Dai, W. Lu, and H. L. W. Chan, J. Mater. Sci. **44**, 5143 (2009).
[13] G. V. Duong, R. S. Turtelli, and R. Groessinger, J. Magn. Magn. Mater. **322**, 1581 (2010).
[14] H. Zheng, J. Wang, S. E. Lofland, Z. Ma, L. Mohaddes-Ardabili, T. Zhao, L. Salamanca-Riba, S. R. Shinde, S. B. Ogale, F. Bai, D. Viehland, Y. Jia, D. G. Schlom, M. Wuttig, A. Roytburd, and R. Ramesh, Science **303**, 661

(2004).
[15] D. Ghosh, H. Han, J. C. Nino, G. Subhash, and J. L. Jones, J. Am. Ceram. Soc. **95**, 2504 (2012).
[16] C. S. Antoniak, D. Schmitz, P. Borisov, F. M. F. D. Groot, S. Stienen, A. Warland, B. Krumme, R. Feyerherm, E. Dudzik, and W. K. H. Wende, Nat. Com. **4**, 1 (2013).
[17] C. X. Li, B. Yang, S. T. Zhang, R. Zhang, Y. Sun, H. J. Zhang, and W. W. Cao, J. Am. Ceram. Soc. **97**, 816 (2014).
[18] S. Haffer, C. Luder, T. Walther, R. Koferstein, S. G. Ebbinghaus, and M. Tiemann, Micro. Meso. Mater. **196**, 300 (2014).
[19] S. Ren, M. Laver, and M. Wuttig, Appl. Phys. Lett. **95**, 153504 (2009).
[20] T. Maiti, R. Guo, and A. S. Bhalla, J. Appl. Phys. **100**, 114109 (2006).
[21] D. Viehland, J. F. Li, S. J. Jang, L. E. Cross, and M. Wuttig, Phys. Rev. B **43**, 8316 (1991).
[22] D. P. Pham, H. T. Nguyen, B. T. Phan, V. D. Hoang, S. Maenosono, and C. V. Tran, Thin Solid Films **583**, 201 (2015).